JOURNAL OF MATERIALS SCIENCE 20 (1985) 316–330

The effect of explosive loading on the microstructure of some metals and alloys

K. E. AEBERLI*, P. L. PRATT
Department of Metallurgy and Materials Science, Imperial College of Science and Technology, Prince Consort Road, London SW7 2BP, UK

The effects of explosive pulses on the microstructure of Al–4.5 % Cu duralumin, tough pitch copper, pure magnetic iron and 18 chromium 8 nickel stainless steel have been studied using transmission electron microscopy. An explosive loading assembly was designed to investigate the effect of both the flanks and the length of shock pulses on the material microstructure. In copper and duralumin it was found that the microhardness increased with the duration of the rarefaction flank. The size of the shock transformed α' martensite particles in stainless steel also increased with rarefaction time. Three wave interactions could be related to the microstructure of baratol-loaded iron and were attributed to the double shock front caused by the α to ϵ phase transformation. Twinning was found to occur when the reflected elastic wave interacted with the first part of the double shock front. The abrupt hardness increase caused by the interaction of the first reflected wave and the second transformation shock front was observed. In addition, a second more gradual hardness increase is attributed to the interaction between the low pressure α and the high pressure ϵ rarefaction waves which caused a relatively slowly increasing rarefaction shock. The microstructure of shocked stainless steel showed that hexagonal ϵ plates and γ twins could occur in the same grain and that α' martensite particles were formed at the intersection of two γ twins, or of ϵ plates and γ twins. Both Kurdjumov–Sachs and Nishyama–Wassermann orientations were observed and sometimes occurred on the same fault band. The short rise and fall times in the pulse flanks made it possible to discuss formation mechanisms for twins and α' martensite particles in terms of the available formation times.

1. Introduction

The transient nature of shock-wave loading requires that any structural changes produced must occur extremely rapidly. If these changes are to be detected they must survive the subsequent rarefaction back to atmospheric pressure, the residual temperature due to adiabatic expansion from the shock temperature and pressure and the deceleration during recovery [1].

The passage of a stable shock wave through a material involves a change of state which occurs within approximately 10^{-9} sec. The abrupt density change is accompanied by the homogeneous generation of large numbers of dislocations in the shock front which accommodate the mismatch between the shocked and unshocked medium. If, as suggested by Meyers [2], the newly generated dislocations achieve considerable velocities due to their mutual repulsion, they will also generate further dislocations but by the more usual multiplication methods.

Under the large shock pressures used, the material undergoes a change from one-dimensional to three-dimensional loading on the passage of the shock front. The pressure is hydrostatic and there appears to be no reason why dislocations should move during this constant pressure period. However, many of the point defects created by the

*Present address: GKSS, Geesthacht, D-2054, West Germany.

0022–2461/85 $03.00 + .12 © *1985 Chapman and Hall Ltd.*

rapidly moving dislocations in the shock front would be annihilated at the high shock temperatures and pressures. The increase in density in the shock pulse can be achieved by a reduction in the existing lattice dimensions or by a transformation to a higher density phase, but not by the creation of vacancies or dislocations, which lead to a decrease in density. Thus a reduction of the dislocation and point defect densities should occur during the high pressure part of the shock pulse, leading to a slight relaxation of the shock pressure.

The shock pressure is reduced to zero by the passage of the rarefaction wave. This is an envelope of the individual pressure release waves, travelling at sonic velocities which correspond to the existing material pressure. Thus all release wave velocities are sonic and considerable dislocation motion should take place. Maximum rarefaction times of between 0.1 and 0.2 μsec would occur in the specimens tested in this work. In these tests the rarefaction times vary linearly between zero at the specimen free surface and a maximum at the shocked surface. Thus the greatest dislocation motion should occur at the shocked surface. These rapidly moving dislocations are responsible for the generation of large numbers of excess point defects and dislocations whose concentration after unloading would depend on the adiabatic release temperature.

Some early investigators tended to ignore the shape of the shock pulse, quoting only the peak pressure and the explosive assembly. This produced a wide variety of structural effects under ostensibly identical conditions. Murr and Kuhlmann-Wilsdorf [3] demonstrated that while increasing shock pressure increased the number of dislocations in shock-loaded nickel, increasing shock pulse duration simply allowed the dislocations to rearrange into better defined cell structures with no appreciable increase in hardness. It seems important to relate the residual structures to the individual characteristics of the shock pulse including the rise time, the peak pressure and duration and the rarefaction tail. In this paper results are presented which attempt to do this for well-characterized shock waves with a number of metals and alloys.

2. Experimental techniques

2.1. The explosive loading assembly

An explosive loading assembly was designed to apply a shock pulse to a thin circular specimen in such a way as to ensure that loading and unloading occurred in opposite directions along the loading axis before rarefaction waves could reach the specimen from the remaining free surfaces of the assembly.

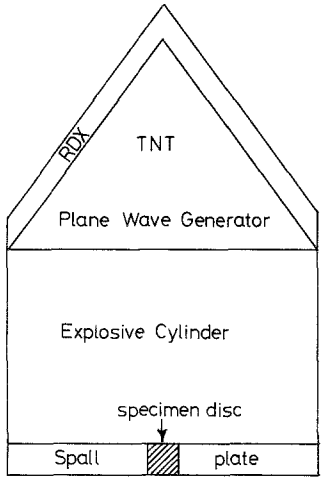

Figure 1 Shock loading assembly with plane wave generator, explosive cylinder and specimen plate.

The assembly, Fig. 1, consisted of an explosive charge comprising a plane wave generator in contact with an explosive cylinder, and a specimen plate made up of a circular spall plate into which was fitted a central specimen disc. The plate surfaces were polished to 1 μm and the plate was attached to the explosive cylinder using a little grease. To obtain a range of shock pressures, three different explosives were used for the cylinder, with the same type of plane wave generator.

The dimensions of the explosive charge and the metal specimen were determined by the requirement that the pressure applied at the explosive–metal interface be constant until the shock front and all of the ensuing rarefaction waves from the specimen surface have traversed the specimen. In other words the pressure should remain roughly constant until it is reduced by the free surface rarefaction waves reaching the explosive–metal interface. Rarefaction waves coming from the circumference of the spall plate and the explosive cylinder as well as those from the plane wave generator, should not reach the specimen until the above sequence has been completed. In this way the specimen could be subjected to a pressure pulse of known magnitude and direction whose duration varied from zero at the free surface of the specimen to a maximum at the explosive–metal interface.

TABLE I Specimen pressures

Explosive	P(GPa)			
	Al–4.5 %Cu	Cu	Fe–18Cr–8Ni	Fe
Baratol	19.0	25.6	25.6	24.8
Composition B	32.1	42.6	42.6	41.3
95 % HMX	41.9	56.7	56.7	55.0

The dimensions of the explosive charge and the specimen plate were calculated using the Rankine–Hugoniot conservation equations for a shock wave [4, 5] combined with the Hugoniot equations of state for the various metals and alloys [6] and the Chapman–Jouguet parameters of the explosive cylinders [7] used in this work. A plane-wave generator 76.2 mm in diamter was attached to an explosive cylinder 50.8 mm thick. The spall plate was 3.2 mm thick and contained a central specimen disc 12.7 mm in diameter.

Four metals and alloys (overaged duralumin Al–4.5 %Cu, tough pitch copper, pure magnetic iron, and 18 Cr–8Ni stainless steel) and three explosives (baratol, cast composition B, and 95 % HMX) were used. The shock pressures are given in Table I. As the Hugoniot and the Chapman–Jouguet data were taken from the literature a series of separate tests was undertaken to check their accuracy. A laser velocity interferometer designed by Amery [8] and based on the VISAR of Barker and Hollenbach [9] was used to determine the free surface velocity and the shock wave velocity.

The measured and calculated shock wave velocities agreed to within 2 % but, whereas the free surface velocities agreed closely under baratol loading, the difference between them increased up to 20 % under HMX loading. This was probably because at these pressures (>50 GPa) the free surface velocity is no longer equal to twice the particle velocity [10].

A series of high speed photographs was taken of the explosive events. This verified that the central specimen discs had not fragmented up to 50 μsec after the onset of plate motion thus indicating the absence of spalling. The discs were slowed down and recovered from a water tank at the end of the experiment as shown in Fig. 2. At the higher shock pressures fragmentation of the discs occurred; this was caused by the deceleration of the specimens in the recovery assembly. The free surfaces of a fragmented duralumin spall plate with the complete specimen disc are shown in Fig. 3.

2.2. The Hopkinson bar impact loading assembly

A split Hopkinson bar 35.1 mm in diameter designed by Yeung-Wye-Kong [11] was used to compress specimens 3.2 mm thick to permanent strains greater than 50 %. These specimens were used to provide a comparison at lower strain rates and pressures with the shocked specimens. The impact bar velocity and the transmitted bar strain data were used to provide stress–strain loading curves for each specimen.

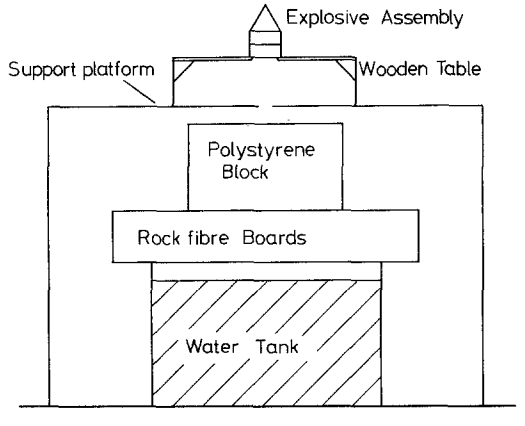

Figure 2 Apparatus for the deceleration and recovery of specimens after shock loading.

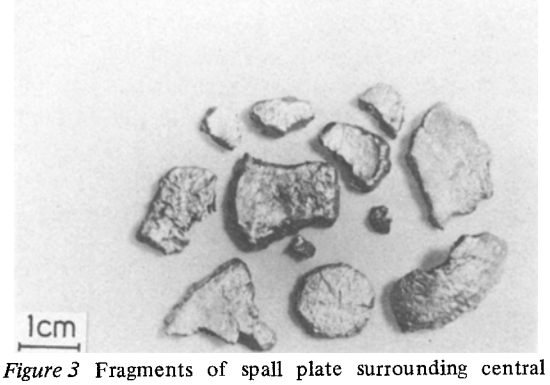

Figure 3 Fragments of spall plate surrounding central specimen disc of baratol-loaded duralumin.

TABLE II Condition of recovered central discs

	Al–4.5 %Cu	Cu	Fe–18Cr–8Ni	Fe
Baratol	Complete	Complete	Complete	Complete
Composition B	Destroyed	Fragments	Complete	Fragments
95 % HMX	-	Destroyed	Complete but damaged	Fragments

2.3. Sample preparation for microstructural examination

After loading, 3 mm cylinders were spark machined from the recovered specimen discs. Where possible, the cylinders were sliced into sections which were ground to thicknesses suitable for jet thinning. The sections sliced from the undamaged shock-loaded discs were used to provide a microstructural traverse across the specimen from the shocked surface to the free surface. In this way it was possible to observe the effect of the pulse length and/or rarefaction stress rate.

A Streuers Tenupol jet thinning machine was used to provide foils for transmission electron microscopy which was carried out using a Phillips EM301, 100 kV electron microscope.

After the removal of the 3 mm cylinders the remains of the specimen discs were sectioned perpendicular to their faces, polished and etched. Microhardness traverses were run perpendicular to the loaded faces of the discs and these were compared with the hardnesses of the as-received material.

3. Experimental results

The condition of the central specimen discs recovered after explosive loading is given in Table II.

3.1. Microhardness measurements

Microhardness values for the as-received, impact and shock-loaded specimens are listed in Table III. Where two or more numbers are given for one test, the first was taken near to the free surface and the last at the shocked surface. In the case of baratol-loaded iron the values correspond to three plateaux. These plateaux and the hardness traverses across the baratol-loaded copper and duralumin discs are shown in Fig. 4a. There was considerable scatter in the hardness of the 18–8 steel (± 10 %) due to the local variations in phase content after loading.

The hardness of the baratol-loaded copper and duralumin show a gradual increase from the free surface to the shocked surface. In baratol-loaded iron (Fig. 4b) the first hardness level (VH 125) exists up to 0.55 mm from the free surface. There follows an abrupt rise to VH 187 which does not change for the next 0.85 mm. From this point the hardness rises erratically within the next 0.6 mm to VH 224 after which it remains roughly constant up to the shocked surface.

The remaining hardnesses listed in Table III are averages taken where no trends were observed.

3.2. Microstructure

3.2.1. Duralumin

The as-received alloy contained evenly distributed spherical precipitates of $CuAl_2$ and easily resolvable dislocations. After impact loading to a strain of 0.75 individual dislocations were no longer resolvable and a cellular structure was formed. No shear bands were observed.

A scan across the baratol-loaded disc revealed bands of dislocations lying on {1 1 1} planes. There appeared to be a gradual increase in the definition of the bands and in their frequency with decreasing distance from the shocked surface whereas a more cellular structure was found in regions further away from the shocked surface. A mixture of isolated slip bands and a few groups of narrow shear bands was found near to the free surface.

The fragments of the plate loaded with compo-

TABLE III Hardness values of as-received, impact and shock-loaded specimens

	Al–4.5 %Cu	Cu	Fe–18Cr–8Ni	Fe
As-received	120	87	277	118
Impact	152	114	348	167
Baratol	138–160	87–115	302	125,187,224
Composition B	122	95	305	172
95 % HMX	–	87	302	177

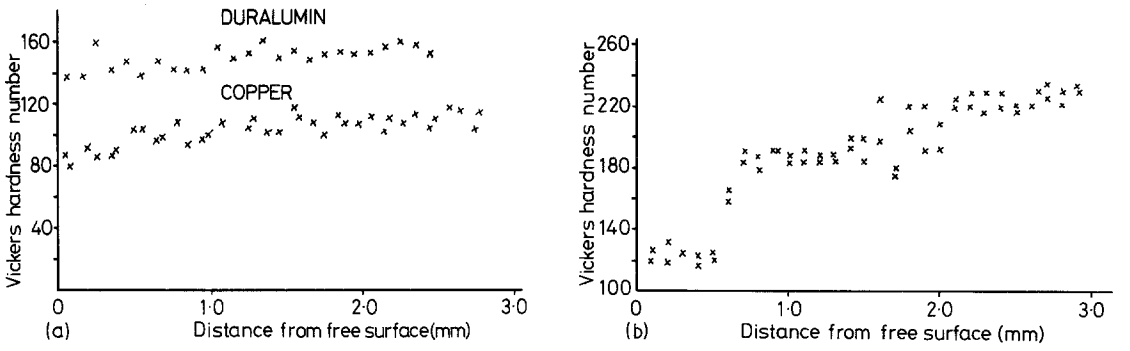

Figure 4 (a) Microhardness traverse across the baratol-loaded copper and duralumin discs. (b) Microhardness traverse across the baratol-loaded iron disc.

sition B contained large numbers of shear bands which ran in up to three different directions. These were similar to those occurring in the baratol-loaded spall plate fragments. There was no significant variation in the precipitate size.

3.2.2. Copper

The as-received copper contained elongated dislocation cells approximately 0.6 μm in width, as expected from its high hardness value.

After impact loading ($\epsilon = 0.71$) the microstructure contained equiaxed cells 0.2 to 0.5 μm wide, dislocations bands and the occasional long shear band containing fine twins 0.01 μm wide. In a few cases there were isolated regions of recovery and recrystallization.

A structure scan of the baratol-loaded disc showed incompletely formed cells and dense dislocation tangles. In addition bands of thin twins, 0.003 to 0.015 μm wide, were found in all regions except those close to the free and shocked surfaces. Well-defined equiaxed cells were found near to the free surface whereas loops and tangled dislocations occurred near to the shocked surface. The overall dislocation density increased from the free surface to the shocked surface.

Extensive recrystallization was found in the fragments of discs loaded with composition B and HMX. There was considerable grain boundary etching – also noted by Murr and Korbonski in shocked 304 stainless steel [12] – and long straight dislocations were observed running parallel to the annealing twins.

3.2.3. 18–8 Stainless steel

3.2.3.1. General features of microstructure The as-received alloy contained stacking faults, planar dislocation arrays, γ(f c c) twins and α(b c c) grains with rows of untangled dislocations. No ϵ(h c p) phase was detected.

Impact-loaded specimens ($\epsilon = 0.53$) had a heavily deformed structure. The γ grains were heavily twinned and contained large amounts of α'. The γ twins were often bent or fragmented, and only occasionally did α' laths lie within the $\{1\,1\,1\}_\gamma$ bands or twins.

Shock loaded 18–8 steel generally contained a dense distribution of $\{1\,1\,1\}_\gamma$ twins and a few ϵ phase plates on $\{1\,1\,1\}_\gamma$ planes, Fig. 5. α' laths of various sizes were found at fault intersections in most grains, Fig. 6. In some cases the as-received α grains contained $\{1\,1\,2\}_\alpha$ twins.

The α' laths occurred at the intersection of twins with twins or with ϵ plates in both the Nishyama–Wassermann (N–W) and the Kurdjumov–Sachs (K–S) orientations. Both orientations were sometimes observed within the same fault band, Fig. 7, but the K–S orientation was favoured by the longer α' laths.

Small α' laths were confined to the width of a single fault band whereas the larger laths crossed several bands and appeared to have grown in a direction almost parallel with one of the intersecting bands.

Sometimes the laths had grown in two twin-related directions, Fig. 8. There was no internal twinning in the α' laths.

The as-received α grains often contained short $\{1\,1\,2\}_\alpha$ twins after shock loading, Fig. 9a. A "twin sheet" structure was found in specimens loaded with composition B and HMX, Fig. 9b. It is not certain whether these occurred in the as-received α grains or were caused by the meeting of large α' laths.

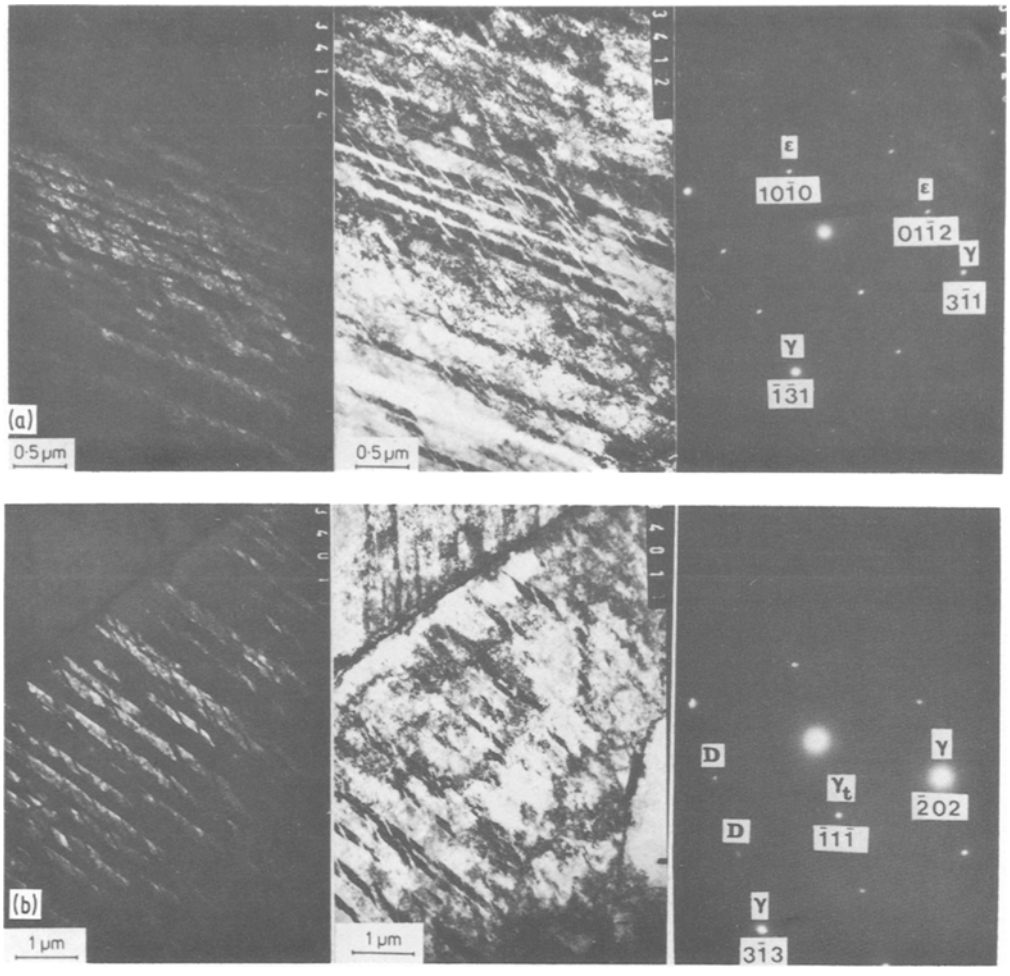

Figure 5 (a) Hexagonal close packed ϵ plates $[\bar{1}\,2\,5]_\gamma \| [\bar{2}\,4\,\bar{3}]_\epsilon$. (b) Face centred cubic γ-twin plates $[1\,6\,1]_\gamma \| [\bar{5}\,\bar{2}\,3]_{\gamma_t}$. For each the dark-field is shown on the left and bright-field in the centre. ϵ = h c p spot; γ = matrix spot; γ_t = twin spot; D = double diffraction spot.

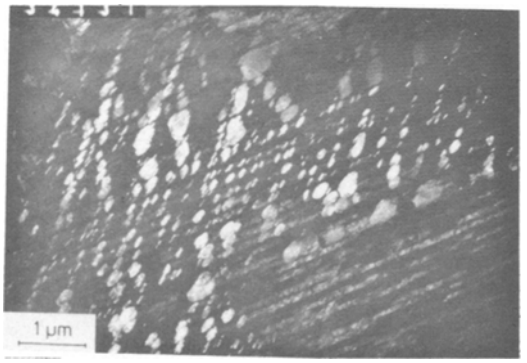

Figure 6 Dark-field micrograph of α' martensite particles. Some ϵ plates can be seen due to the closeness of the ϵ and α' diffraction spots.

3.2.3.2. Change in microstructure with distance from free surface The baratol-loaded disc was heavily faulted with γ twins and some ϵ plates were detected. Close to the free surface the α' phase occurred as small laths lying within the fault bands. As the distance from the free surface increased the laths became larger and began to overlap neighbouring bands to produce elongated crystals. Near to the shocked surface the crystals formed in two, twin-related directions. There was some twinning in the as-received α grains.

The microstructure of the specimen loaded with composition B was also heavily faulted but contained large numbers of overlapping α' laths which often grew in twin-related directions. There

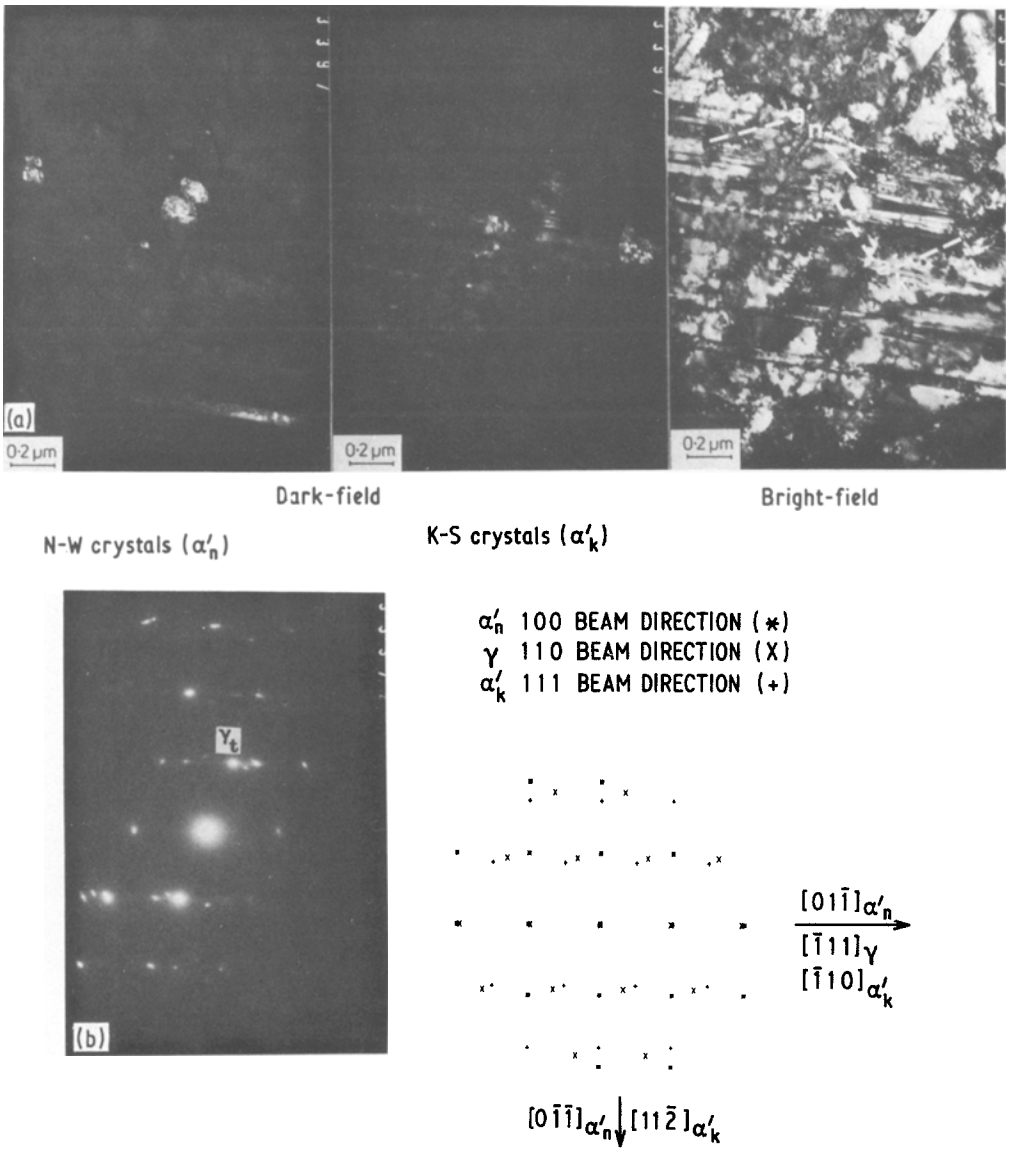

Figure 7 (a) α' martensite crystals in the Nishyama–Wasserman (N–W) and Kurdjumov–Sachs (K–S) orientation. The left-hand and centre micrographs show the dark field and the right-hand shows the bright field. (b) shows the diffraction pattern and computer plot (twin spots not shown). $[1\,1\,0]_\gamma \parallel [1\,0\,0]_{\alpha'_n} \parallel [1\,1\,1]_{\alpha'_k}$. γ_t = twin spot; γ = matrix spot; α'_n = N–W crystals; α'_k = K–S crystals.

was extensive twinning in the as-received grains and the twin sheet structure was observed. No positional variation of the α' lath size across the disc was observed.

The HMX-loaded disc was heavily deformed and the microstructure resembled that of the impact specimen. There was little sign of ϵ plates. The as-received α grains were frequently twinned and the twin sheet structure occurred often. No microstructural trends across the disc were observed.

3.2.4. Pure iron

Optical micrographs of impact-loaded iron etched with 2% nital did not show twinning. Baratol-loaded iron discs produced the typical results of the double (P1, P2) shock front shown in Fig. 10a. The lightly etched untransformed (P1) region extends 0.55 mm in from the free surface, at which point the darkly etched, transformed (P2) region begins. Twinning in the untransformed region does not occur within 0.28 mm of the free surface. Discs shocked with composition B or

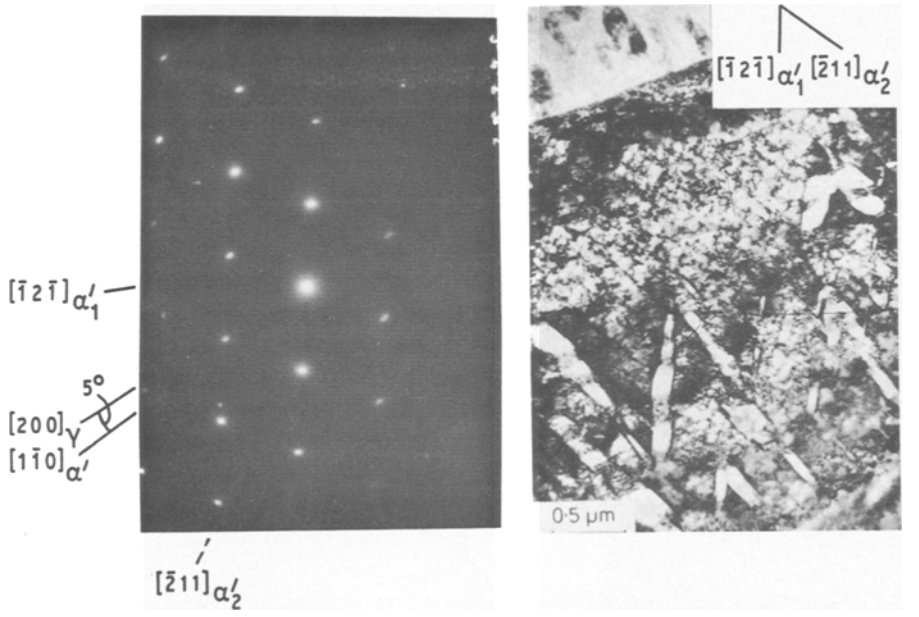

Figure 8 Twin-related α' crystals $[\bar{1}2\bar{1}]_{\alpha'_1}$ direction reflected about $(11\bar{2})_{\alpha'}$ plane to produce $[\bar{2}11]_{\alpha'_2}$. $(011)_\gamma \| (111)_{\alpha'} \| (\bar{1}\bar{1}\bar{1})_{\alpha'_4}$. The right-hand micrograph shows the bright field.

HMX had no untransformed regions because the P2 wave travels faster than the P1 wave. They were darkly etched throughout and, in addition, recrystallized in regions of high strain such as at the free surface.

The positions of the three zones in Fig. 10a permit an analysis of the shock wave profile. The shock profile consists of three successive fronts, Fig. 10b. The leading elastic shock ($P_e = 0.68$ GPa) and the second P1 shock (13 GPa) have velocities which are largely independent of the final loading pressure. These were determined by Bancroft *et al.* [13] and are $U_e = 6.04$ km sec^{-1} and $U_{P1} = 5.05$ km sec^{-1}. The velocity of the third, transformation shock (P2) depends on the final shock pressure and can be determined from the position of the reflected wave R1/P2 interaction, 0.55 mm from free surface.

The position of the interaction between the reflected e-wave (Re) and the P1 wave can be calculated using the equation

$$\frac{U'_{P1}}{U_e} = (1-r)/[1 + (U_e/R_e)r] \qquad (1)$$

developed by Fowler *et al.* [14] where $U'_{P1} = \rho_e/\rho_0(u_{P1} - u_e)$, r is the ratio of the distance between the interaction position and the free surface to the specimen width, R_e is the elastic rarefaction wave velocity, u_{P1} and u_e are the particle velocities after the passage of the P1 and e shocks and ρ_e/ρ_0 is the density ratio across the e shock. Using the values of ρ_e, u_e, R_e, U_e and U_{P1} determined by Bancroft *et al.* [13] in Equation 1 places the interaction position at 0.28 mm from the specimen free surface. This corresponds to the distance from the free surface at which twinning was first seen in Fig. 10a.

4. Discussion

4.1. Effect of annealing upon the microstructure

During shock compression the material temperature rises to a maximum T_H. This value is reduced to T_a after isentropic release to atmospheric pressure. In the case of impact loading, only the temperature generated by isentropic release has a significant value (Table IV). If the microstructure is to reflect shock or impact loading neither the isentropic release temperature nor the rate of cooling from this temperature must lead to microstructural changes. In the case of duralumin, room temperature is above 0.3 T_m and thus considerable recovery must have occurred between loading and examination, although the precipitates in duralumin probably reduced this effect. Similarly, copper would have undergone some intermediate temperature recovery at room temperature. The shocked specimens were quenched from T_a to the water tank temperature within a millisecond of loading,

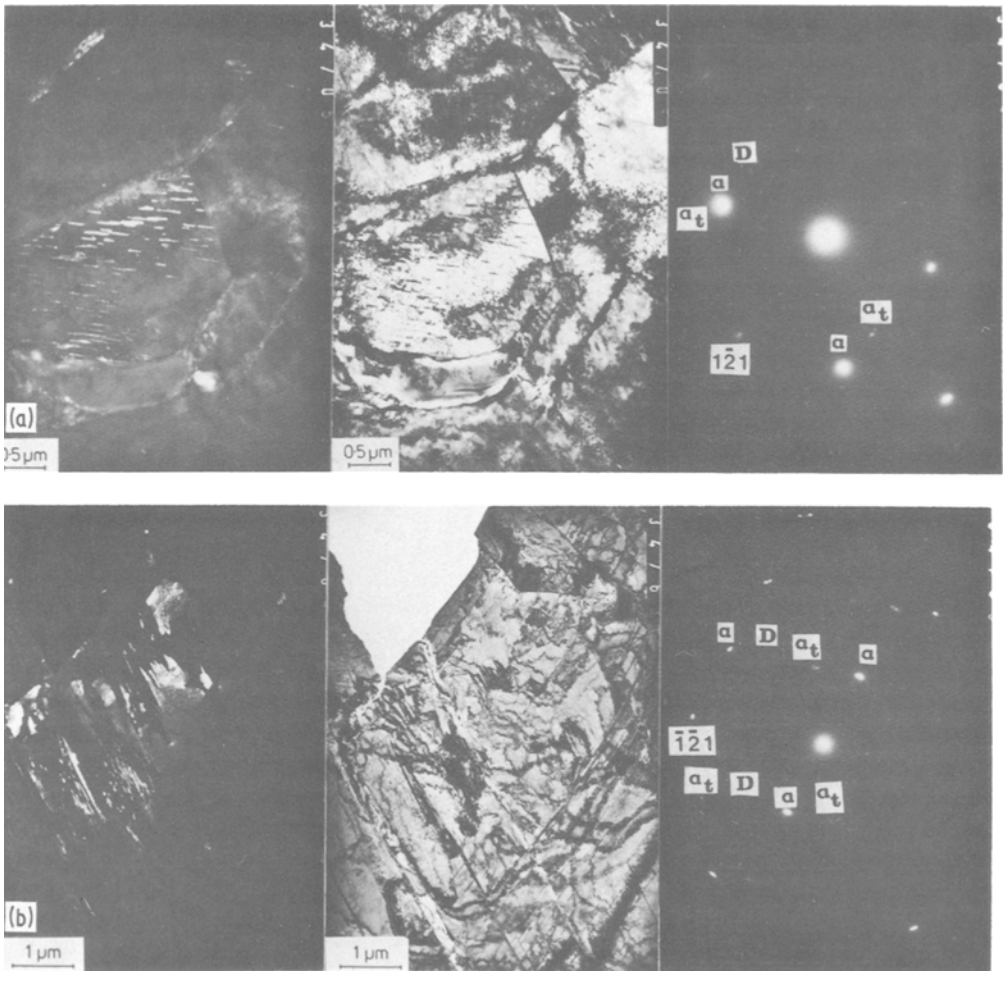

Figure 9 (a) Shock twinning on $[1\,\bar{2}\,1]_\alpha$ twin plane in an as-received α grain. (b) "Twin sheet" structure on $[\bar{1}\,\bar{2}\,\bar{1}]_\alpha$ twin plane in shocked as-received α grains. In (a) $[0\,1\,2]_\alpha \parallel [0\,\bar{1}\,\bar{2}]_{\alpha_t}$, while in (b) $[1\,1\,3]_\alpha \parallel [\bar{1}\,\bar{1}\,\bar{3}]_{\alpha_t}$. α_t = twin spot; α = matrix spot; D = double diffraction spot. The micrographs on the left show the dark-field and those in the centre the bright field.

and the impact specimens cooled in air to room temperature within a few minutes.

The heavily deformed free surfaces of copper and iron loaded by composition B and HMX had recrystallized. The extreme deformation occurring during specimen deceleration is probably responsible for this, although the recrystallization time is unknown. This is supported to some extent by the discovery of recrystallized grains in heavily deformed impact-loaded copper. This problem of the time of recrystallization is highlighted by the work of Cohen *et al.* [15] who showed that

TABLE IV Shock and isentropic release temperatures (T_H, T_a)

	Al–4.5 % Cu			Cu			18–8 Steel			Fe		
	T_H (° C)	T_a (° C)	T_a/T_m*	T_H (° C)	T_a (° C)	T_a/T_m*	T_H (° C)	T_a (° C)	T_a/T_m*	T_H (° C)	T_a (° C)	T_a/T_m*
Hopkinson bar	—	189	0.56	—	112	0.28	—	171	0.25	—	136	0.22
Baratol	217	91	0.44	165	69	0.25	145	57	0.18	190	93	0.20
Composition B	486	212	0.59	352	163	0.32	301	132	0.23	405	213	0.27
95 % HMX	753	329	0.73	560	269	0.40	476	218	0.27	639	343	0.34

*T_m = melting temperature

shock-loaded copper, which was left for several months at room temperature, underwent isolated recrystallization. The absence of recrystallization in impact-loaded iron can be attributed to the low value of T_a/T_m. The 18–8 stainless steel, iron, baratol-loaded copper and to a lesser extent the baratol-loaded duralumin specimen microstructures were probably very similar to those existing immediately after loading.

4.2. Effect of shock loading on the microstructure

The consideration of the residual microstructures after impact and shock loading can be divided into three parts: (a) dislocation structure, (b) twin formation and (c) phase transformations.

4.2.1. Dislocation structure

The results for copper and duralumin shocked with baratol indicate that the hardness increase from the free surface to the shocked surface is accompanied by a corresponding increase in dislocation density. Since the shock rise time and the shock pressure remain constant as the shock wave traverses the specimen, the dislocation density must depend on both the pulse length and the rarefaction time. Whereas an increased pulse length would tend to favour recovery and thus a hardness

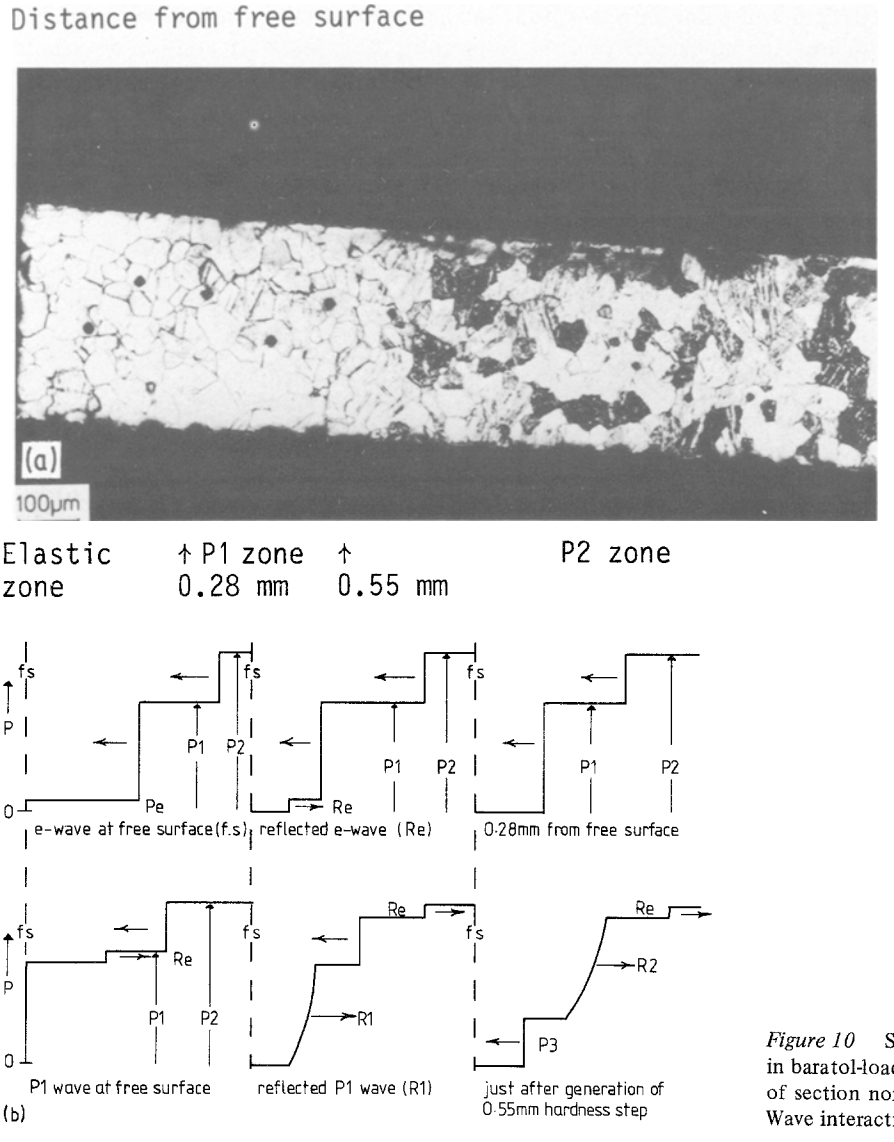

Figure 10 Shock wave interaction in baratol-loaded iron. (a) Micrograph of section normal to free surface. (b) Wave interaction diagrams.

reduction as the shocked surface is neared, increasing rarefaction time would account for the increasing hardness and dislocation density.

Within the rarefaction tail all the dislocations can move and the distance that they move will depend upon the rarefaction time. Thus, assuming an average dislocation velocity of 1 km sec^{-1} in an obstacle-free single crystal, dislocations could move distances varying from zero at the free surface to a few hundred μm at the shocked surface. In the case of baratol-loaded copper and duralumin, the maximum distance would be about 150 μm. Obviously, a typical dislocation would never travel this distance in these heavily dislocated, polycrystalline specimens. However, the longer the rarefaction time, the greater would be the number of new dislocations and point defects produced by sources caused by the interaction of rapidly moving dislocations with obstacles such as other dislocations, grain boundaries, precipitates or twins. The electron micrographs of baratol-loaded copper show incomplete cells, and dislocation loops and tangles. The incomplete cells have been attributed previously to the lack of sufficient time (pulse length) for their formation. Certainly, the 1 μsec maximum pulse length in these experiments is at the low end of the pulse range investigated by Appleton and Waddington [16] and Murr and Kuhlmann-Wilsdorf [3] for shocked copper and nickel respectively. However, even if the pulse length were long enough to permit the dislocations created in the shock front to form a cell structure, there seems little reason to suppose that this would survive the considerable high-speed motion and generation of dislocations occurring during unloading in the rarefaction cell. Thus, the completeness of the dislocation cells should depend on the rarefaction time and, sometimes more importantly, on the value and duration of the isentropic release temperature and the subsequent room temperature behaviour of the microstructure. If cell formation does occur during rarefaction, it is likely to take place at low rarefaction rates (low pressures) when dislocations are moving relatively slowly and few new dislocations are being generated. Thus the incomplete cells found in baratol-loaded copper may be the result of the short rarefaction time (0.16 μsec) and the low isentropic release temperature (0.25 T_m). However, in baratol-loaded duralumin considerable recovery and recrystallization should have occurred since the isentropic release temperature (0.44 T_m) and room temperature (0.33 T_m) are large fractions of the melting point. The hardness values suggest that this has not occurred, which probably reflects the effect of the large precipitate concentration.

The anomalous microstructures found at the free surfaces of the copper and duralumin specimens (well-formed dislocation-free cells in copper and bundles of shear bands in duralumin) were caused by the high strains and high local temperatures occurring during specimen deceleration. This is supported by the occurrence of large numbers of shear bands observed in the heavily deformed fragments of duralumin loaded with composition B. The dislocation loops and tangles in copper in regions close the the shocked surface may have been the result of the von Neumann spike, a shock front in the explosive rising well above the stable shock pressure. This spike lasts only a very short time, being reduced rapidly to the shock pressure by a subsequent rarefaction tail and thus only a small region close to the shocked surface of the specimen would be affected. Micrographs of copper loaded with composition B and HMX show similar features in unrecrystallized regions. This tends to support the above explanation, although the effect of the longer rarefaction tail and the high isentropic release temperatures should not be forgotten.

Finally, the dislocation structure of the heavily deformed impact-loaded copper is compared with that of the lightly deformed baratol-loaded copper at similar values of the hardness. The impact-loaded copper contains dislocation-free, equiaxed, complete cells whereas the baratol-loaded copper contains incomplete cells with few dislocation-free areas. In impact loading the pulse front lasts for about 0.5 msec so that inertial effects can be ignored and loading is at constant volume. The slow rise time does not require the homogeneous generation of dislocations, there being sufficient time for dislocations to move and multiply by more conventional means and for microscopic grain distortion to occur. Also after maximum load is reached there is sufficient time during the constant load period (0.5 msec) for dislocations to form into complete cells. The unloading wave will have far less effect on the microstructure than the shock rarefaction wave and cooling slowly to room temperature from the high adiabatic release temperature would permit some recovery. In the shocked case the high speed dislocations interact to produce large numbers of point defects, jogs

TABLE V Measured twin dimensions and their possible formation times (dislocation velocity $v = 3\,\mathrm{km\,sec^{-1}}$)

	Fe	Cu	γ-SS	α-SS
L (μm)	60	100	0.6–6	0.3
h (μm)	0.25	0.03	0.003–0.08	0.005
No. of atomic planes	2000	150	15–400	45
Dislocation pole (μsec)	0.01	0.02	0.001–0.01	0.00005
Spiral dislocation pole (μsec)	0.1	0.2	0.01–0.10	0.0006
Homogeneous nucleation (μsec)	140	15	0.1–25	0.015

and tangles. Thus subsequent dislocation realignment is more difficult and it must occur at room temperature since the specimen is rapidly quenched in the water tank.

Although similar hardness values occur in specimens subjected to long pulse shock loading and to impact loading, the source of the hardness is different. In impact specimens, hardening is caused by well-formed dislocation cells and grain size reduction in the loading direction, whereas point defects, dislocation jogs, loops and tangles are responsible for the shock-loaded hardness.

4.2.2. Twin formation

Deformation twins in b c c and high stacking fault energy f c c metals and alloys tend to be long and thin, usually running between grain boundaries. Twins in low stacking fault energy metals and alloys are short and often terminate within grains. The reason is thought to be the relative ease of twin nucleation and the velocity of the twinning dislocations when they encounter forest dislocations in their path. In the first case, the twinning dislocation accelerates rapidly so that propagation through forest dislocations is possible and twins only stop at grain boundaries. In the second case, nucleation is easy and dislocation acceleration is low, thus enabling forest dislocations to halt twinning dislocations [17–19]. The micrographs of iron and copper show that the twins formed are indeed long and thin, relatively infrequent, and stopped only by grain boundaries and sometimes, in the case of iron, by other twins. However, in γ stainless steel, long unbroken twins are also seen completely traversing grains, although most of the twins are short and often imperfect. The twins in α stainless steel appear to begin and end within the α grains, but apparently not at intersections with other twins (cf. γ-stainless steel).

Dislocation motion and multiplication is confined largely to the shock front and the rarefaction tail. The times required for twin formation by the pole mechanism and by homogeneous nucleation (see Appendix) are given, together with the typical twin lengths and widths, in Table V. If these are compared with the rise time of the shock pulse (0.001 μsec) and the fall time of the rarefaction tail (0.1 to 0.2 μsec maximum) some general observations can be made.

(i) The straight dislocation pole model could not apply to copper, iron or γ-stainless steel twins as the formation times are too long.

(ii) If the twins were formed during the shock front they would most likely be the result of homogeneous nucleation and their concentration would be independent of their position in the specimens. However, the twinning times for copper and iron appear to be too long even for homogeneous nucleation and thus it is possible that no shock front twins form in these cases.

(iii) The spiral pole mechanism could only operate successfully during the rarefaction tail (with the possible exception of the α-stainless steel). In this case the average twin length might be expected to increase with distance from the specimen free surface, leading to a preference for short twins between grain boundaries nearer to the free surface and a mixture of short and longer twins nearer to the shocked surface.

The question arises as to what happens to twins which do not reach the grain boundaries due to lack of time. In the absence of an applied force, the twin would attempt to contract, the degree of contraction being dependent on the obstacles in its path. The apparent absence of short twins starting and/or ending within copper or iron grains suggests that either complete untwinning occurs (this would seem unlikely as considerable dislocation motion must have occurred inside and outside the twinned region), or else the pole mechanism is not responsible for twinning. This conclusion cannot be made in the case of γ-twinning in stainless steel since twins are terminated not only by grain boundaries but also by other twins or bands within the grains. Thus twinning could have been caused by the pole mechanism, although the plentiful supply of stack-

ing faults seems to favour an overlapping mechanism. α-twinning in stainless steel provides an interesting comparison with twinning in pure iron. The α twins are short, thin and of reasonably constant length. They do not appear to start or end on other twin or slip planes (cf. γ twins). Thus their lengths are determined either by the available twinning time or by dislocation tangles which, in contrast to those in pure iron, would have to be capable of stopping twinning dislocations. In the former case, twinning would have to have occurred within the shock front by means of a pole mechanism, as the α twins would have been considerably longer had they been formed in the rarefaction tail or by homogeneous nucleation. In the latter case, the dislocation density in the α grains would have to be considerably higher than that in pure iron, or the nucleation stresses much lower.

Finally, consideration should be given to the twin nucleation stress. If this forms a substantial fraction of the maximum load difference in the flanks of the shock pulse, the available twin propagation time would be considerably reduced. Thus twins would be shorter. However, this is not the case in copper, which twins at impact loads, or in γ-stainless steel. In pure iron, twinning does not occur at impact loads but does occur at a 13 GPa shock pressure (P1). The calculated position of the interaction between the reflected elastic wave and the P1 shock front corresponds almost exactly to the onset of twinning in baratol-loaded iron. Thus, twinning appears to nucleate during rarefaction from 13 GPa to about 12.3 GPa, giving considerable scope for twin growth during the remainder of the rarefaction tail.

In conclusion, homogeneous twin nucleation appears to be more likely in copper and γ-stainless steel (either in the shock front or the rarefaction tail) and in iron (in the rarefaction tail), whereas the pole mechanism appears more likely in α-stainless steel (in the shock front).

4.2.3. Phase transformations

Both iron and stainless steel undergo pressure-induced phase transformations. This is evidenced by the hardness step in baratol-loaded iron and the existence of α' and ϵ phases in the residual microstructure of the stainless steel.

4.2.3.1. Iron In iron, the high pressure ϵ phase transforms back to α'-martensite on unloading and hence its occurrence can only be detected by the

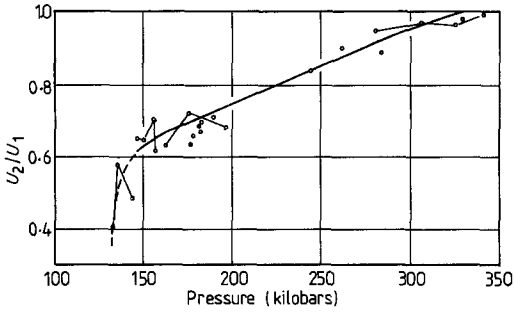

Figure 11 Graph of P2 and P1 shock velocity ratio U_2/U_1 against shock pressure (Smith and Fowler [20]).

effect of the double shock front on both the microhardness (Fig. 4b) and the etching characteristics (Fig. 10a). The resulting step changes were only observed at the lowest shock pressure (25 GPa, baratol). At the higher loading pressures (41 GPa, comp.B and 55 GPa, HMX) the P2 transformation wave travels faster than the P1 wave, thus generating only one shock front (P2). This is confirmed by the absence of hardness steps in these specimens.

In the baratol-loaded specimen the value of U_{P1}/U_{P2} determined from the position of the interaction between the reflected P1 wave (R1) and the oncoming P2 wave lies somewhat below the curve of Smith and Fowler [20], Fig. 11. This suggests that the actual P2 pressure may have been as low as 21 GPa, although Smith and Fowler's results do show considerable scatter.

The hardness measurements (Fig. 4) show a second, more gradual, rise after the initial step in a region between 1.4 mm and 2.0 mm from the free surface. Calculations (Fig. 12) show that the reflected P3 wave (R3) catches up with the R2 rarefaction wave in this region. The leading part of the reflected wave overtakes the R2 wave at about 1.4 mm whereas the trailing part overtakes it at

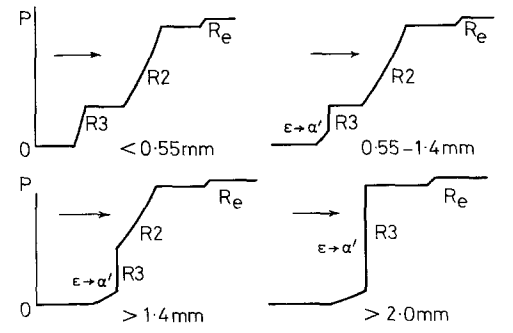

Figure 12 Tensile wave interactions. (*Distances are measured from the free surface).

about 2.0 mm. This leads to an increase in the pressure drop between 1.4 mm and 2.0 mm from the free surface. Now the pressure of the P3 wave is greater than 8.1 GPa which means that the ϵ to α' transformation does not occur until the R3 rarefaction wave passes through the transformed iron. On reflection from the free surface, the R3 wave provides a gradual rarefaction to atmospheric pressure. However, when it reaches the high pressure ϵ phase at 0.55 mm from the free surface it causes the $\epsilon \rightarrow \alpha'$ phase change. The wave shape changes to a rarefaction shock from the P3 pressure to 4.5 GPa followed by a gradual rarefaction to the atmospheric pressure. This transformation shock will produce a hardness increase which remains constant until the R3 wave catches up to the R2 wave at 1.4 mm from the free surface. From this point until 2.0 mm from the free surface, the rarefaction shock increases from about 4 GPa to about 20 GPa. Thus, the driving forces for the transformation will be increased considerably and hence the deformation and hardness will increase. Beyond 2.0 mm the rarefaction shock is constant and no further hardness increase occurs.

Finally, the hardness of the composition B and HMX-loaded specimens are less than that of the transformed baratol-loaded specimen, reflecting probably some degree of recovery.

4.2.3.2. 18–8 stainless steel The absence of any hardness steps in the explosively loaded specimens indicates the absence of a two-wave structure at these pressures. This was also noted by Fowler *et al.* [14] in their shock tests on commercial 18–8 steel containing up to 40 % α phase. However, two points should be mentioned. Firstly, ϵ plates have been detected under conventional, low strain rate loading conditions indicating a very low transformation stress relative to that in iron. Secondly, the density change for the $\gamma \rightarrow \epsilon$ transformation in 18–8 steel is about -0.81 % compared to an estimated -5.9 % for the $\alpha \rightarrow \epsilon$ transformation in iron [21, 22]. Thus the break in the Hugoniot curve, and hence the pressure range for a possible double shock formation, would both be considerably less for stainless steel than for iron. Therefore it is not surprising that a two-wave structure is absent at the pressures used here.

The absence of the ϵ phase in impact-loaded specimens ($\epsilon = 0.52$) is in agreement with the results of Bowkett and Harries [21] who showed that the ϵ phase ceases to exist in 18–8 EN 58 B stainless steel cold-rolled to greater than 50 % deformation.

The scarcity of ϵ plates in shock-loaded 18–8 stainless steel may be due to the reported tendency of ϵ to revert back to γ at temperatures above 150° C [21]. This temperature is exceeded (albeit for a short time) at these pressures and, in conjunction with the expected $\epsilon \rightarrow \alpha'$ transformation and the relatively high stacking fault energy, this may explain the absence of ϵ plates.

The ϵ and/or γ_t to α' transformation is thought to occur by stress or pressure relief. Under the uniaxial loads provided by the Hopkinson bar, the α' phase can form by the continuous relief of highly-stressed ϵ–ϵ and ϵ–γ_t intersections. Thus α' could occur at any time during the load pulse. In the shock case, the pressure is hydrostatic and thus transformations will occur during the rarefaction tail. As the results show, the amount of transformation product occurring in shocked specimens is considerably less than that in impact-loaded specimens reflecting the short shock pulse time.

Since α' formation results from the movement of transformation dislocations which only occurs during the rarefaction tail, it might be expected that the length or size of the α' laths would reflect the length of the rarefaction tail at any point in the specimen. This appears to be the case in baratol-loaded 18–8 steel but is not obvious at composition B or HMX pressures.

Due to the widely varying shapes of these α' laths and insufficient knowledge concerning their growth mechanism, no attempt was made to correlate lath length and rarefaction tail length. However, some type of pole mechanism would seem to be responsible for α' growth, as a rough calculation shows that an overlap mechanism would require less than 10^{-9} sec to generate the longest α' laths. Thus either the α' lath growth is limited by obstructions such as dislocations, twins or other grains (which is not supported by the findings of this work or by those of Murr and co-workers [23, 24]), or else lath growth occurs by some mechanism which slows the growth time to the 10^{-7} sec available within the rarefaction tail (e.g. pole mechanism).

In conclusion, the absence of a double shock wave structure may be due to the low $\gamma \rightarrow \epsilon$ transformation pressure and the small density charge involved. Thus at the shock pressures employed, the P2 wave moves faster than the P1 wave. The α' phase appears to form within the rarefaction tail

and the size of the α' laths shows some dependence on the length of the rarefaction tail. The transformation sequence is probably:

$\gamma \rightarrow \gamma_t$	+	$\epsilon \rightarrow \alpha'$
During shock front		During rarefraction tail

Acknowledgements

The authors wish to thank the Department of Mechanical Engineering, Leeds University, for the use of the Hopkinson bar impact loading facility, the Directors of RARDE and AWRE for the provision of experimental facilities for shock loading, and the SRC and RARDE for financial support for KEA.

Appendix

Considering a twin of thickness h and length L, the formation times t_t are as follows:

A.1. Pole Mechanism

(i) Straight dislocation of length $L/2$ sweeps out equal areas during each revolution.

$$t_t = \frac{h\pi L}{dv}$$

where d is the habit plane spacing and v the dislocation velocity [25].

(ii) Dislocation takes on the shape of an Archimedes spiral which forms a twin whose oblateness (h/L) depends on the applied stress [26].

$$t_t = \frac{2\pi L}{v}$$

A.2. Homogeneous nucleation

Large numbers of overlapping dislocation loops generated at the same time grow to radius $L/2$.

$$t_t = \frac{L}{2v}$$

These are minimum times and assume that the twin nucleus was at a point halfway along the final twin length. Obviously, if twin growth is halted in any direction by an obstacle, the final value of L will no longer reflect the formation time.

References

1. K. E. AEBERLI, Ph.D. Thesis, University of London, (1982).
2. M. A. MEYERS, *Scripta Metall.* **12** (1978) 21.
3. L. E. MURR and D. KUHLMANN-WILSDORF, *Acta. Metall.* **26** (1978) 847.
4. W. J. M. RANKINE, *Phil. Trans. Roy. Soc. (London)* **160** (1870) 277.
5. H. HUGONIOT, *Compt. Rend. Acad. Sci.* **101** (1885) 1118, 1229.
6. R. KINSLOW, "High Velocity Impact Phenomena" (Academic Press, New York, 1970).
7. K. BURROWS, D. K. CHILVERS, R. GYTON, B. D. LAMBOURN and A. A. WALLACE, 6th Symposium on Detonation, AC-R-221 (Office of Naval Research, Department of the Navy, Arlington, VA, 1976) p. 625.
8. B. T. AMERY, 6th Symposium on Detonation, AC-R-221 (Office of Naval Research, Department of the Navy, Arlington, VA, 1976) p. 673.
9. L. M. BARKER and R. E. HOLLENBACH, *J. Appl. Phys.* **43** (1972) 4669.
10. M. H. RICE, R. G. McQUEEN and J. M. WALSH, "Solid State Physics, Advances in Research and Applications", Vol. 6 (Academic Press, New York, 1958) p. 1.
11. Y. C. T. YEUNG-WYE-KONG, Ph.D Thesis, University of Leeds, (1972).
12. L. E. MURR and J. A. KORBONSKI, *Met. Trans.* **1** (1970) 3333.
13. D. BANCROFT, E. L. PETERSON and F. S. MINSHALL, *J. Appl. Phys.* **27** (1956) 291.
14. C. M. FOWLER, F. S. MINSHALL and E. G. ZUKAS, Metals Society Conference No. 9, "Response of Metals to High Velocity Deformation", Estes Park, 1960, (Interscience Publishers, New York, 1961) p. 275.
15. J. B. COHEN, A. NELSON and R. J. De ANGELIS, *Trans. AIME* **236** (1966) 133.
16. A. S. APPLETON and J. S. WADDINGTON, *Acta Metall.* **12** (1964) 956.
17. D. G. WESTLAKE, Proceedings of the AIME-IMD Conference on Deformation Twinning, 1964, edited by R. E. Reed-Hill (Gordon and Breach Publishers, New York, 1964) p. 29.
18. J. A. VENABLES, Proceedings of the AIME-IMD Conference on Deformation Twinning, 1964 p. 77.
19. D. HULL, Proceedings of the AIME-IMD Conference on Deformation Twinning, 1964 p. 121.
20. C. S. SMITH and C. M. FOWLER, Metals Society Conference No. 9, "Response of Metals to High Velocity Deformation", Estes Park, 1960, (Interscience Publishers, New York, 1961) p. 309.
21. W. W. BOWKETT and D. R. HARRIES, Harwell Report AERE-R-9093 (1978).
22. R. L. WOODWARD and R. L. AGHAN, *Metals Forum* **1**(4) (1978) 180.
23. L. E. MURR and K. P. STAUDHAMMER, *Mater. Sci. Eng.* **20** (1975) 35.
24. L. E. MURR, E. MOIN, K. WONGWIWAT and K. P. STAUDHAMMER, *Scripta Metall.* **12** (1978) 425.
25. J. B. COHEN and J. WEERTMAN, *Acta Metall.* **11** (1963) 996.
26. J. FRIEDEL, "Dislocations" (Pergamon Press, London, 1964) p. 182.

Received 5 March
and accepted 13 March 1984